**Geomechanics and Engineering**, *Vol. 23, No. 6 (2020) 535-546*
DOI: https://doi.org/10.12989/gae.2020.23.6.535


# Study on the mechanical properties and rheological model of an anchored rock mass under creep-fatigue loading

Yang Song[1a] and Yong qi Li*[2]

[1]*Department of Architecture and Transportation, Liaoning Technical University, 47 Zhonghua Road, Fuxin, Liaoning Province 123000, China*
[2]*Department of Civil Engineering, Liaoning Technical University, 47 Zhonghua Road, Fuxin, Liaoning Province 123000, China*

*(Received October 10, 2020, Revised December 10, 2020, Accepted December 14, 2020)*

**Abstract.** The stress environment of deep rock masses is complex. Under the action of earthquakes or blasting, the strength and stability of anchored rock masses in fracture zones or faults are affected. To explore the variation in anchored rock masses under creep-fatigue loading, shear creep comparative testing of anchored marble specimens with or without fatigue loading is performed. Considering the damage variable of rock under fatigue loading, a rheological model is established to characterize the whole shear creep process of anchored rock masses under creep-fatigue loading. The results show that (1) the overall deformation of marble under creep-fatigue loading is larger than that under only shear creep loading, and the average deformation is increased by 18.3%. (2) By comparing the creep curves with and without fatigue loading, the two curves basically coincide when the first level stress is applied, and the two curves are stable with the increase in stress level. The results show that the strain difference among the specimens increases gradually in the steady-state stage and reaches the maximum at the fourth level. (3) The shear creep is described by considering the creep mechanical properties of anchored rock masses under fatigue loading. The accuracy of this creep-fatigue model is verified by laboratory tests, and the applicability of the model is illustrated by the fitting parameter $R^2$. The proposed model provides a theoretical basis for the study of anchored rock masses under low-frequency earthquakes or blasting and new methods for the stability and reinforcement of rock masses.

**Keywords:** anchored rock mass; fatigue load; shear creep; accelerating element; creep-fatigue model

## 1. Introduction

In recent years, with the rapid economic development of our country, some large-scale deep rock mass projects related to improving the national economy and individual's livelihood have been implemented. For example, the Sichuan-Tibet Railway will include dozens of ultra-long and ultra-deep tunnels with a length of approximately 10 km and a burial depth of more than 1000 m. Earthquakes occur frequently along this railway, and the corresponding fault fracture zone is dense (Xue *et al.* 2020, Kılıc *et al.* 2002). How to ensure the safety and stability of the sections of deeply buried tunnel crossing the fault fracture zone under the action of earthquakes needs to be addressed. At present, deep resource mining, large-scale hydropower projects in the central and western regions, and the excavation of underground strategic oil reserves generally utilize blasting methods. The blasting disturbance is extremely destructive to the surrounding rock support structure (Chen *et al.* 2018, Wang *et al.* 2019). How to ensure that the rock will remain stable during blasting disturbance also needs to be addressed. With the gradual extension of geotechnical engineering from shallow to deep, deep rock masses are facing a complex environment of "three highs and one disturbance" (Griggs 1939, Song *et al.* 2020), and surrounding rock and roadway support maintenance face many challenges. The stress state of deep surrounding rock is close to the ultimate bearing strength of the rock mass. Earthquakes and engineering blasting both induce dynamic and low-cycle cyclic loads, which are important causes of surrounding rock deformation (Chen *et al.* 2016, Wang *et al.* 2020). Therefore, studying the creep mechanical properties of anchored jointed rock masses under low-cycle cyclic loading has not only great theoretical value but also significant engineering guiding significance for the support of surrounding rock and roadways under earthquake and blasting factors (Tadeusiewicz 2015, Jiang *et al.* 2017).

Studying the deformation and failure of a rock mass under the action of cyclic loading and unloading is very important to reveal the failure mechanism of the deep rock mass. Scholars in China and abroad have carried out a series of studies for this purpose: Bagde and Petroš (2005) studied how the loading waveform and amplitude influenced the fatigue performance of intact sandstone through dynamic uniaxial cyclic loading tests on sandstone; the relationship between the energy released from the sandstone samples and loading frequency and amplitude was obtained, which is useful for revealing the behavior of rock masses in excavation systems under cyclic loading and thus has practical meaning. Liu and Li (2018) studied the

*Corresponding author, Ph.D. Student
E-mail: liyongqi9@126.com
[a]Professor
E-mail: lgdsongyang@163.com



ISSN: 2005-307X (Print), 2092-6219 (Online)

Table 1 Conventional mechanical parameters of marble

| Compressive strength/MPa | Elastic modulus/GPa | Poisson's ratio | Cohesion/MPa | Internal friction angle/(°) | Shear strength/MPa | Tangential stiffness/GPa·m |
|---|---|---|---|---|---|---|
| 120.00 | 20.20 | 0.28 | 2.61 | 33.50 | 20.6 | 3.20 |

mesoscale damage characteristics of rock samples under cyclic loading and unloading with the particle flow software PFC and performed conventional triaxial compression laboratory tests on marble to obtain data that can truly reflect the macroscopic mechanical properties of marble mesoscale parameters. Meng *et al.* (2016) revealed the energy evolution of rock deformation and failure by studying the characteristics of energy accumulation, evolution and dissipation of uniaxial cyclic loading and unloading compression under different loading rates (Choi *et al.* 2019).

To study the rheological properties of rock masses under low-cycle cyclic loading, scholars have established corresponding rheological models to describe the rheological properties of cyclic loading and unloading rock masses by introducing nonlinear elements and other methods. Wang *et al.* (2019) in order to study the nonlinear creep characteristics and creep disturbance effects of deep rock under the action of perturbation load, carried out uniaxial compression perturbation tests of rock under static axial pressure, different perturbation amplitudes and different perturbation frequencies. By combining the results of these creep tests and nonlinear viscoplastic perturbation creep components and damage components, a composite model of nonlinear perturbation creep damage was established for rock. Tang *et al.* (2019) established the creep theory model of granite residual soil based on rheological theory and the creep characteristics of granite residual soil under different stress levels and obtained the dynamic behavior of granite residual soil under cyclic loading by derivation to propose a theoretical model of stress accumulation. Yang *et al.* (2018) proposed a granite fatigue constitutive model based on internal variables by conducting experiments and theoretical analyses on the cyclic loading of granite under different confining pressures and different peak deviator stresses. The verification shows that the model can better reflect rock fatigue mechanics in nature. Xu and Yang (2015) based on the triaxial cyclic loading and unloading creep testing of rock, carried out effective viscoelastic-plastic strain separation of the creep strain of the sample and obtained a viscoelastic-plastic creep model of rock. Their study showed that the model can be very effective and provide a good description of the elastoplastic loading and elastic unloading creep characteristics of a sample under a cyclic loading and unloading path.

The above studies mainly focus on the analysis of uniaxial compression creep and triaxial compression creep under cyclic loading and unloading. There are few studies on the variation in the strength of deep anchored rock masses under shear creep stress conditions suddenly subjected to a low-frequency earthquake or blasting load, that is, a small amount of the research on shear creep focused on anchored rock masses under creep-fatigue loads. In this paper, low-cycle cyclic loading is used to simulate fatigue loading, equivalent to a low-frequency earthquake or blasting disturbance, and a shear creep test of marble under creep-fatigue loading is carried out, and the influence of the creep-fatigue load on shear creep of the anchored rock mass is studied. By introducing a nonlinear acceleration element to describe the shear creep of an anchored rock mass and considering the disturbance effect of a fatigue load on the anchored rock mass, a constitutive model describing the whole process of shear creep of an anchored rock mass under a creep-fatigue load is established. The accuracy of the model is verified by comparing the theoretical model with experimental data, which reflect the effect of low-frequency earthquakes or blasting loads on deep rock masses. The results of the study provide some ideas.

## 2. Introduction to the test

### *2.1 Test scheme*

In this test, marble from a mine roadway in Fuxin, Liaoning Province, is selected as the test specimen, the main reason why marble is selected as a typical elastic-plastic rock lie in the fact that it can better describe the typical creep characteristics of rock, and its strength is easy to be processed into the test specimen. The basic mechanical parameters, such as the compressive strength and the elastic modulus of marble materials, need to be determined before the shear test. Through the uniaxial compression test, the triaxial compression test, and the direct shear test, the basic mechanical parameters of the marble are determined, and the average value of the marble test data is taken as the test result, and its conventional mechanical parameters are shown in Table 1.

A low-cycle cyclic load is used to simulate the fatigue load, and shear creep comparative testing is carried out with or without the fatigue load, that is, whether to increase the effect of the low-cycle cyclic load is considered in the process of shear creep loading. The loading path of the low-cycle cyclic load is shown in Fig. 1.

The test is divided into four comparative test groups: 1, 2, 3 and 4. Each comparative test group includes IA and IB (I = 1, 2, 3, 4). The properties of the two specimens are consistent during the manufacturing process. The control group 1A-4A corresponds to the anchored rock mass shear creep testing without the low-cycle cyclic load, the test group 1B-4B corresponds to the anchored rock mass shear creep testing with the low-cycle cyclic load, and the control group does not undergo the shear stress. Apart from the different loading paths, the other conditions of the corresponding specimens are kept the same. The specific test scheme is shown in Table 2.

### *2.2 Specimen fabrication and test equipment*

#### *2.2.1 Specimen fabrication*

Marble from the Haizhou open-pit mine was selected for

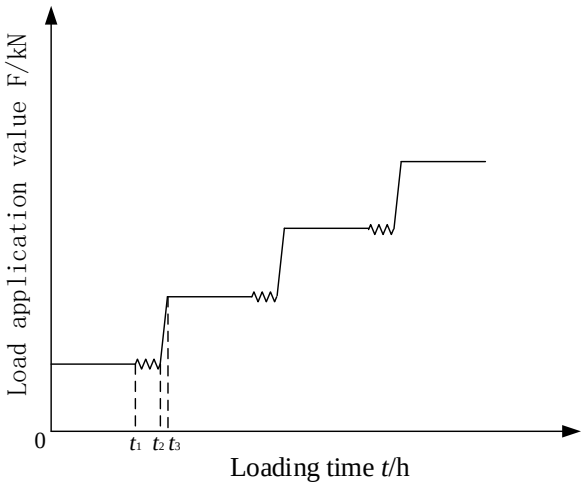


Fig. 1 Loading path diagram Note: time 0-$t_1$ in the Fig. 1 represents the stable stage of load application, which corresponds to 59 h; $t_1$-$t_2$ represents the low-cycle cyclic loading stage of the load, i.e., the simulated fatigue load, which is applied for 0.5 h;$t_2$-$t_3$ represents the reapplication stage of the load, which is applied for 0.005 h

Table 2 Test scheme

| Test group | Shear stress/MPa |
|---|---|
| Control group | 24—48—72—96 |
| Experimental group | 24—(24.5~23.5)—48(48.5~47.5)—72—(72.5~71.5)—96 |

Note: the maximum and minimum values of the low-cycle cyclic load are shown in parentheses to indicate the variation in the low-cycle cyclic load stress. When the low-cycle cyclic load stress fluctuates between the maximum value and the minimum value, the duration from the original shear stress to the maximum or minimum value and then back to the original shear stress is 0.005 h, a loading and unloading cycle is 0.01 h, and each cycle loading and unloading has 50 cycles, for a total test duration of 5 h

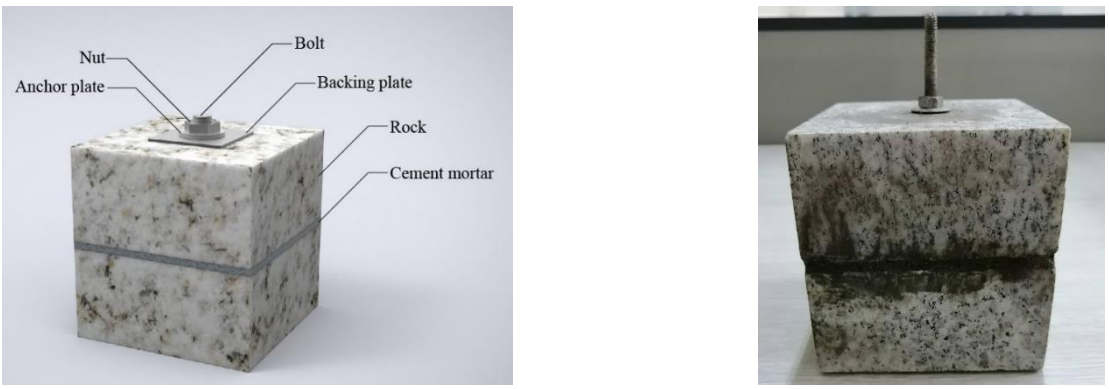


(a) Model diagram (b) Photograph

Fig. 2 A test piece

this test. The test pieces were all 100 mm × 100 mm × 100 mm cubes. The size of the test pieces conformed to the relevant provisions of the test specifications of the international society of rock mechanics (Scheuermann 1978). The methods and devices applied in the test meet the relevant requirements and standards of the international rock mechanics, the relevant production steps of the test pieces were as follows:

(1) Rock block processing: The block marble is selected, and the rock block is processed into dimensions of 100 mm × 100 mm × 50 mm by a rock cutting machine. A hole with a diameter of 10 mm and a length of 50 mm is drilled along the center of the rock mass from one of the 100 mm × 100 mm sides for the anchor rod.

(2) Rock block bonding: Cement mortar is used to bond the upper and lower plates of a rock block. The cement mortar is poured into the 100 mm × 100 mm × 5 mm cuboid to create a joint thickness of 5 mm. The joint cement mortar mix ratio is cement:river sand:water = 1:1.5:0.8. The test materials are 42.5 ordinary Portland cement and medium sand. The joint shape, size and material ratio are ensured during the test. The indoor curing time is 28 days.

(3) Installation of the anchor rod: HRB335 steel with a yield strength of 335 MPa is selected as the anchor material.

Table 3 Technical performance indicators of the equipment

| Number | Parameter | Unit | Value |
|---|---|---|---|
| 1 | Overall stiffness of the testing machine | GN/m | >10 |
| 2 | Maximum axial load | kN | 2000 |
| 3 | Effective force measuring range | kN | 40-2000 |
| 4 | Measuring force resolution | N | 20 |
| 5 | Accuracy of force measurement | % | ±1 |
| 6 | Maximum confining pressure applied | MPa | 100 |
| 7 | Accuracy control of confining pressure | % | ±2 |
| 8 | Sample size | mm | Φ100×100 |
| 9 | Maximum shear test value | kN | 1000 |
| 10 | Shear displacement to piston | mm | 100 |
| 11 | Temperature control range | ℃ | -40~200 |

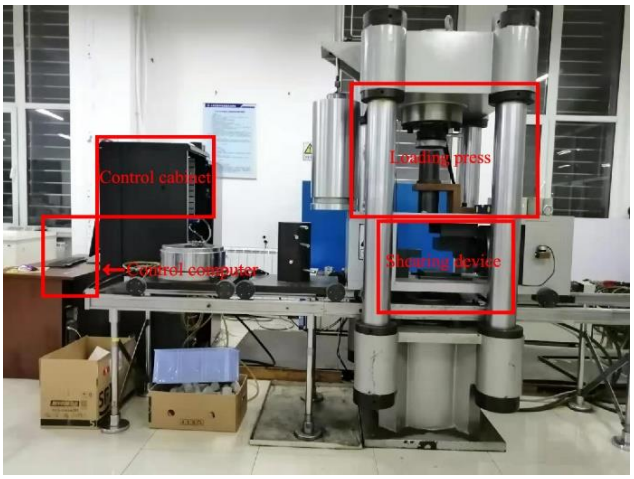


Fig. 3 Shearing device

A steel bar with a diameter of 6 mm is installed into the hole previously drilled into the test piece. The overall length of the reinforcement is 110 mm. One end of the ribbed steel bar is machined with a length of 10 mm, and the remaining length is 50 mm deep into the upper and lower walls. Grouting is used to fill the relevant holes to reinforce the anchor rod. The material is consistent with the joint material.

An anchored jointed rock mass produced according to these steps is shown in Fig. 2.

#### 2.2.2 Test equipment

The test loading system adopts the cutting equipment of the TAW-2000 triaxial testing servo apparatus of the civil engineering test center of Liaoning University of Engineering and Technology. As shown in Fig. 3, the TAW-2000 testing machine is composed of a loading system, measuring system, controller and other parts. It adopts microcomputer-controlled electrohydraulic servo valve loading and manual hydraulic loading to complete automatic control. The loading press and control cabinet are separate, and the testing machine collects stress and displacement data. Various test curves are collected automatically by the host computer, and the reliability of the test results is high. The TAW-2000 electro-hydraulic servo rock triaxial testing machine have the ability to automatically complete the rocks' uniaxial and triaxial compression tests, uniaxial & triaxial rheological tests, and shear composite tests. In the test, the electro-hydraulic servo proportional valve group with wide range of speed regulation and computer digital control is applied to automatically and accurately realize the tests of the axial and radial constant stress, the constant strain, and the constant displacement. It can dynamically display the whole process of the test (such as test force, confining pressure, axial deformation, and radial deformation). Moreover, it can also collect, store, process, and display test data and test curve in real time, and print test report. The test machine parameters are shown in Table 3.

### 2.3 Test procedure and results

#### 2.3.1 Test procedure

The test is carried out by graded loading (Jorat *et al.* 2013; Ajamzadeh *et al.* 2019). First, the compressive strength of the specimen is obtained through the conventional mechanical test to determine the shear stress to apply at each level. The test is divided into four levels of loading, which are 20%, 40%, 60% and 80% of the compressive strength of the specimen. This test is an unconfined shear creep test, and the test steps for each test group are as follows:

(1) Application of shear stress: The anchored rock mass is put into the shear device, and then the load is controlled with the control rate of 0.5 MPa/s, and the horizontal shear stress is incrementally applied. After each stage of loading is applied, the load is kept constant, and the instantaneous displacement is measured and recorded.

(2) Application of low-cycle cyclic load: When each level of shear stress is applied, at approximately 59 h, the specimen is controlled by displacement and applied with a 1 kN/s loading and unloading rate. The amplitude of the low-cycle cyclic shear load of each level is 1/10-1/100 of the compressive strength. The shear stress level is rapidly increased and maintained for approximately 0.005 h. Then, the shear stress level is reduced and maintained for approximately 0.005 h, and this cycle is repeated 50 times. Before and after the beginning of low-cycle cyclic loading, the pressure is stabilized for a period of time, and the internal stress of the specimen is adjusted to make it more in line with engineering practice. See Fig. 1 and Table 2 for details.

(3) Read data: The attenuation and steady-state shear creep values are recorded at 5 min, 10 min, 20 min, 40 min, 1 h, 2 h, 4 h, 8 h, and 12 h and then again at 12 h intervals (Nield *et al.* 2014; Kılıc *et al.* 2003). Additionally, when the specimens are subjected to low-cycle cyclic loading, the data are read every 0.5 min, and each level of load is maintained for approximately 60 h. The stable condition of shear creep deformation of a rock mass is creep when the rate increment is $\leq 5 \times 10^{-4}$ mm/D. During the accelerated creep stage, considering the larger creep deformation and faster creep time, the data are read every 5 min until the specimen is damaged.

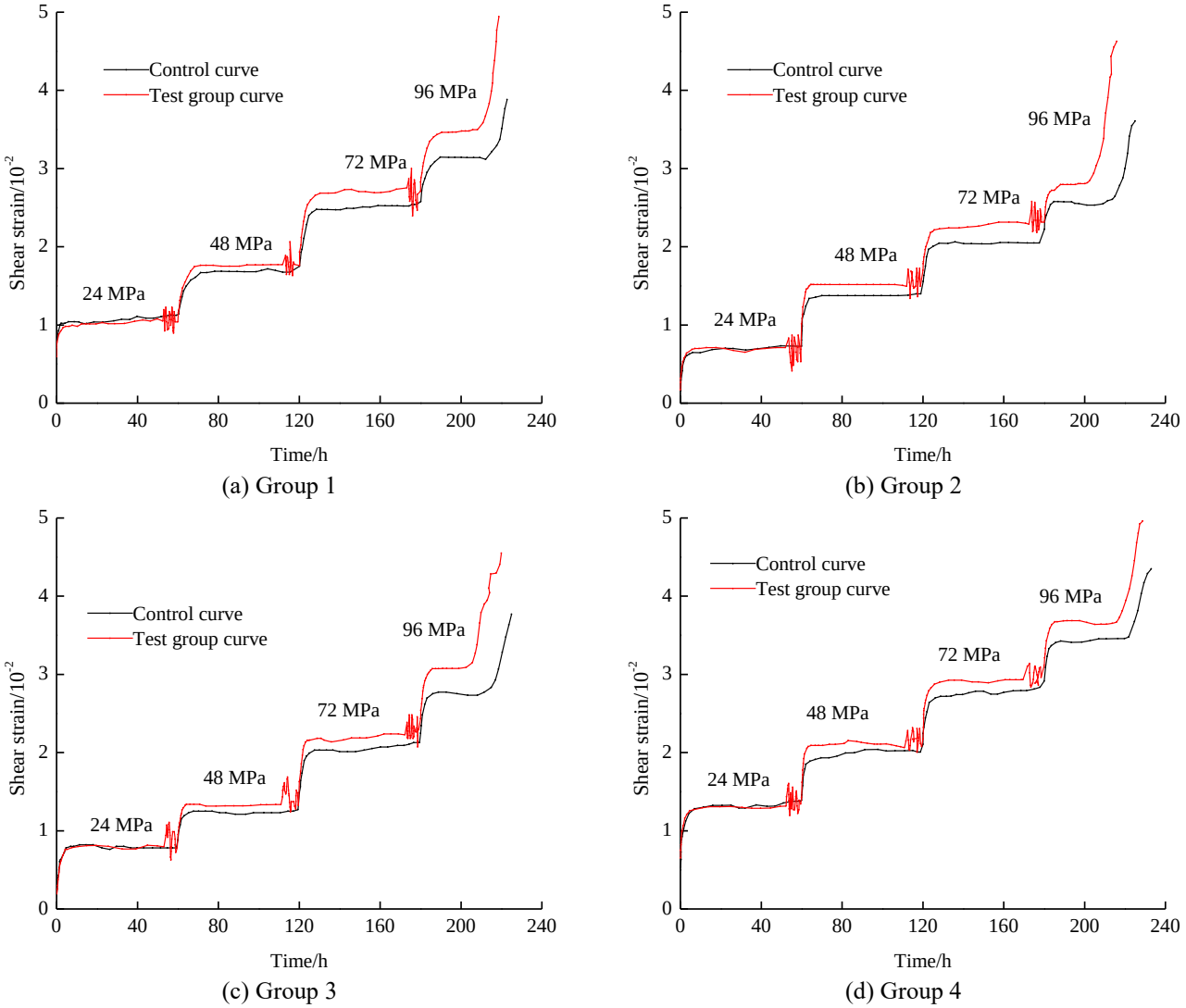


Fig. 4 Test curves

Table 4 Strain summary table

| Group | Specimen number | Total strain $\varepsilon/10^{-2}$ | Incremental strain at all levels $\Delta\varepsilon_i/10^{-2}$ | | | | Strain increment coefficient $K$/% | | | |
|---|---|---|---|---|---|---|---|---|---|---|
| | | | First level | Second level | Third level | Fourth level | First level | Second level | Third level | Fourth level |
| Group 1 | 1A | 3.884 | 0.551 | 0.729 | 0.886 | 1.423 | 14.2 | 18.8 | 22.8 | 36.6 |
| | 1B | 4.942 | 0.475 | 0.730 | 0.907 | 2.133 | 9.6 | 14.8 | 18.4 | 43.2 |
| Group 2 | 2A | 3.607 | 0.493 | 0.571 | 0.591 | 1.383 | 13.7 | 15.8 | 16.4 | 38.3 |
| | 2B | 4.626 | 0.531 | 0.571 | 0.669 | 2.343 | 11.5 | 12.3 | 14.5 | 50.6 |
| Group 3 | 3A | 3.769 | 0.391 | 0.625 | 0.644 | 1.524 | 10.4 | 16.6 | 17.1 | 40.4 |
| | 3B | 4.550 | 0.412 | 0.628 | 0.628 | 2.157 | 9.1 | 13.8 | 13.8 | 47.4 |
| Group 4 | 4A | 4.348 | 0.669 | 0.728 | 0.735 | 1.434 | 15.4 | 16.7 | 16.9 | 33.0 |
| | 4B | 4.962 | 0.647 | 0.745 | 0.764 | 1.882 | 13.0 | 15.0 | 15.4 | 37.9 |

The experimental steps of the control group included only steps (1) and (3).

### *2.3.2 Test results*

By analyzing the test data, the test curves of the test group and the control group were obtained, as shown in Fig. 4.

### *2.3.3 Analysis of test results*

To study the influence of a creep-fatigue load on the shear mechanical properties of an anchored rock mass, the shear strain increments of specimens under different grades are summarized, and the ratio of the incremental strain to total strain at all levels is defined as the strain increment coefficient K to quantitatively explain the influence degree

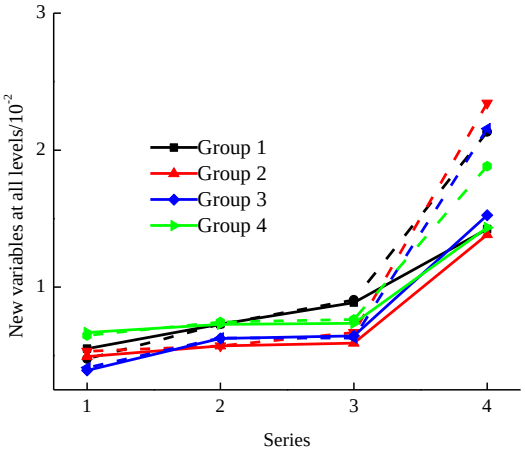


Fig. 5 Creep strain increment at all levels Note: the solid line corresponds to the control group, and the dotted line corresponds to the test group

of the creep-fatigue load at all the levels of strain tested, as shown in Fig. 5 and Table 4.

(1) In terms of total strain, the deformation of specimens under a creep-fatigue load is larger than that of specimens without a creep-fatigue load, with an average increase of 18.3%; the largest difference is observed with the first group, with an increases of 22%, and the smallest difference is observed with the fourth group, with an increase of 12.4%.

(2) According to the strain increment of each level, the deformation of group changes slightly among levels 1-3. The deformation increases rapidly when the stress reaches the fourth level. The specimen does not undergo large deformation until the fourth level because under the first three levels, the original pores in the specimen close while new pores form and gradually connect. When the fourth level is reached, the internal pores of the specimen undergo creep. A comparison of the creep-fatigue load curves show that the curves of the control and test groups basically coincide. With the increase in level, the strain difference among specimens in the steady-state phase increases gradually, and the curve gap increases gradually. At the fourth level, the strain difference reaches the maximum.

(3) Fig. 5 indicates that the creep-fatigue load has a positive effect on the shear deformation of a specimen and that the deformation is larger than that of the corresponding specimen tested without creep-fatigue load. This result arises because the creep-fatigue load disturbs the shear creep specimen to a certain extent, which accelerates the development of pores and cracks in the specimen, and the interlayer dislocation becomes obvious. The results show that the first three stages of creep-fatigue loading cannot be fully applied to the specimen, as part of the load the specimen. Finally, in the accelerated creep stage, the specimen deformation is no longer restrained, resulting in an increase in specimen deformation.

## 3. Creep-fatigue model

The shear creep curve of a rock mass mainly includes

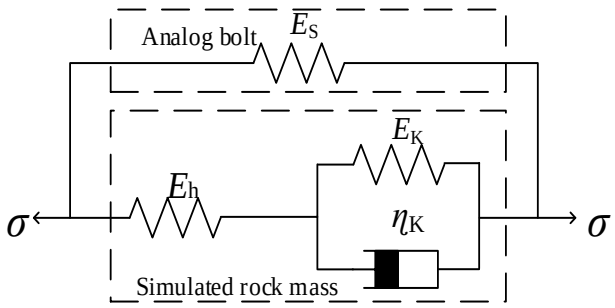


Fig. 6 Linear model of anchored rock mass

the attenuation creep stage, stable creep stage and accelerated creep stage. The above analysis shows that the creep-fatigue shear test curve of the anchored rock mass also includes the abovementioned stages; however, the shear creep curve of an anchored rock mass rises under creep-fatigue load, and at the end of the first three stress levels, the creep-fatigue test curve is applied. The results show that the shear strain-time curve shows irregular fluctuation under the load, which results in a large degree of deformation of the specimen in the failure stage, which indicates that the influence of creep-fatigue load on the shear deformation of an anchored rock mass is obvious and mainly concentrated in the acceleration stage. Therefore, it is necessary to conduct mechanical analysis on the shear deformation of anchored rock masses under creep-fatigue load.

### 3.1 Linear model of anchored rock mass

The creep curve of the rock mass under shear exhibits attenuation and steady-state stages. At present, the Burgers model or generalized Kelvin model are commonly used to describe these two stages. The Burgers model can reflect the growth of deformation with time in the steady-state creep stage, which is suitable for describing the creep characteristics of soft rock, while the creep rate of the steady-state stage in the generalized Kelvin model is almost 0, which is suitable for hard rock (Vásárhelyi and Ván. 2006). Therefore, in this paper, the generalized Kelvin model is used to describe the decay and steady-state stages of marble. Considering the anchoring of the jointed rock mass with the anchor bolt, the description of the anchor bolt as an elastic body (Tang *et al.* 2019), and the coupling effect and deformation coordination of an anchored rock mass, the generalized Kelvin model and elastic element are used to reflect the attenuation and steady-state stages of an anchored rock mass. The model diagram is shown in Fig. 6, and its constitutive equation is as follows:

$$\frac{\eta_k}{E_h+E_k}\dot{\sigma}+\sigma=\frac{E_hE_k+E_hE_s+E_sE_k}{E_h+E_k}\varepsilon+\frac{\eta_k(E_s+E_h)}{E_h+E_k}\dot{\varepsilon} \quad (1)$$

where σ is the stress, $\varepsilon$ is the strain, $E_s$, $E_h$ and $E_k$ are the elastic moduli of the corresponding element, and $\eta_k$ is the viscosity coefficient.

### 3.2 Acceleration element

The main reason for the nonlinear shear rheology of a

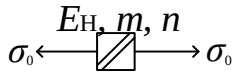


Fig. 7 Acceleration element

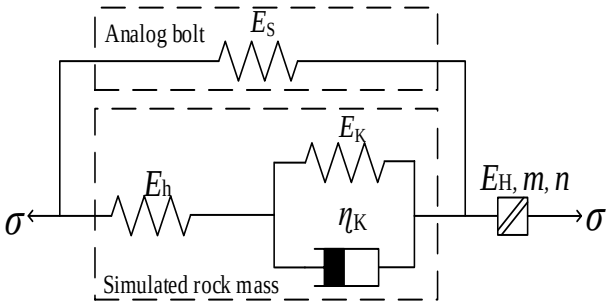


Fig. 8 Rheological model of anchored rock mass

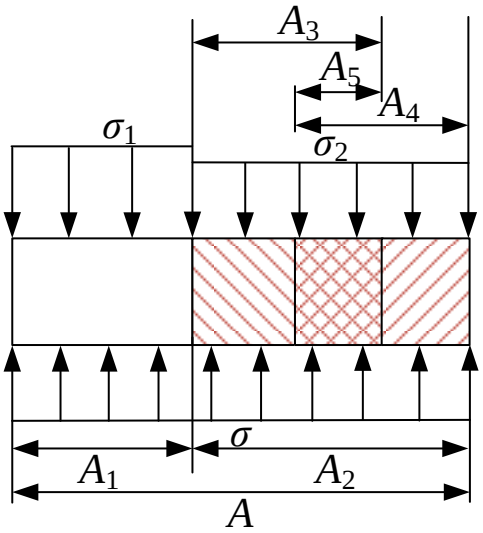


Fig. 9 Axial stress diagram of rock microelement

rock mass is that under the creep-fatigue load, microcracks existing in the rock mass will undergo a process of accelerated propagation with the effect of the creep load and time. Therefore, it is considered that the nonlinear shear rheological deformation of a rock mass is a function of time (Choi *et al.* 2019). Therefore, we modify the original nonlinear rheological element (NRC element) (Yang *et al.* 2007)by introducing an acceleration factor M to obtain a new accelerating element that can reflect the nonlinear change of an anchored rock mass during the acceleration stage of shear creep. As shown in Fig. 7, this element is abbreviated as body *E*, and its corresponding creep equation is as follows:

$$\varepsilon = \frac{\sigma}{E_{\mathrm{H}}}\{1 - m \times \exp[-(\frac{t - t_{\mathrm{s}}}{t_{\mathrm{p}} - t_{\mathrm{s}}})^{n}]\} \tag{2}$$

where σ is the stress; $\varepsilon$ is the strain; $E_{\mathrm{H}}$, $m$ and $n$ are the rheological parameters of the model, where $m$ is the acceleration factor and $n$ is the failure factor; $t$s is the transition time from the steady-state stage to the acceleration stage; and $t$p is the shear failure time of the rock mass. Notably, Eq. (2) is valid when $t>t_{\mathrm{s}}$ because it considers the nonlinear change in the rock mass during the acceleration stage of shear creep.

### 3.3 Rheological model of anchored rock mass

According to the above analysis, a rheological model describing the whole shear creep process of an anchored rock mass is obtained by connecting the linear model of an anchored rock mass with the improved NRC acceleration element in series. As shown in Fig. 8, the constitutive equation is as follows:

(1) When $t \le t_{\mathrm{s}}$, the model is transformed into the linear model of a bolted rock mass shown in Fig. 6, which is used to describe the attenuation and steady-state stage of shear creep of the anchored rock mass, and $\sigma=\sigma_0$ is introduced into Eq. (1) to obtain:

$$\dot{\varepsilon} + \frac{E_{\mathrm{h}}E_{\mathrm{k}} + E_{\mathrm{h}}E_{\mathrm{s}} + E_{\mathrm{s}}E_{\mathrm{k}}}{\eta_{\mathrm{k}}(E_{\mathrm{s}} + E_{\mathrm{h}})}\varepsilon = \frac{E_{\mathrm{h}} + E_{\mathrm{k}}}{\eta_{\mathrm{k}}(E_{\mathrm{s}} + E_{\mathrm{h}})}\sigma \tag{3}$$

The corresponding creep equation is:

$$\varepsilon(t) = \exp(-Pt) * [C + \frac{Q}{P}\exp(Pt)] \tag{4}$$

where $P = \frac{E_{\mathrm{h}}E_{\mathrm{k}} + E_{\mathrm{h}}E_{\mathrm{s}} + E_{\mathrm{s}}E_{\mathrm{k}}}{\eta_{\mathrm{k}}(E_{\mathrm{s}} + E_{\mathrm{h}})}$, $Q = \frac{E_{\mathrm{h}} + E_{\mathrm{k}}}{\eta_{\mathrm{k}}(E_{\mathrm{s}} + E_{\mathrm{h}})}$.

When t=0, the instantaneous elastic deformation of the anchor is $\varepsilon_0 = \frac{\sigma_0}{E_{\mathrm{h}} + E_{\mathrm{s}}}$, and by substituting this into Eq. (4), we obtain $C = \frac{\sigma_0}{E_{\mathrm{h}} + E_{\mathrm{s}}} - \frac{Q}{P}$.

(2) When $t>t_{\mathrm{s}}$, the model is the rheological model of an anchored rock mass, which is used to describe the whole process of shear creep of an anchored jointed rock mass, including the acceleration stage. The corresponding creep state equation is:

$$\varepsilon(t) = \exp(-Pt) * [C + \frac{Q}{P}\exp(Pt)] + \frac{\sigma}{E_{\mathrm{H}}}\{1 - m \times \exp[-(\frac{t - t_{\mathrm{s}}}{t_{\mathrm{p}} - t_{\mathrm{s}}})^{n}]\} \tag{5}$$

### 3.4 Creep-fatigue model

The shear damage of an anchored rock mass under creep-fatigue load includes the undamaged part, damage under the shear creep load, damage under the fatigue load, and damage under the combined action of the creep load and fatigue load. The force on a rock microelement is shown in Fig. 9:

In the figure above, $A$ is the total area of the rock mass; $A_1$ is the undamaged area of the rock mass; $A_2$ is the damaged area of the rock mass; $A_3$ is the damaged area of the rock mass under the shear creep load; $A_4$ is the damaged area of the rock mass under the fatigue load; $A_5$ is the damaged area of the rock mass under the combined action of the shear creep load and the fatigue load; $\sigma$ is the nominal stress borne by the rock mass; $\sigma_1$ is the effective stress

Table 5 Summary of model parameters

| Specimen number | Shear stress/MPa | $E_h$/GPa | $E_k$/GPa | $E_s$/ GPa | $\eta_k$/MPa·h | $E_H$/GPa | $m$ | $n$ | $D$ | $R^2$ |
|---|---|---|---|---|---|---|---|---|---|---|
| 1B | 24 | 1.47 | 2.41 | 11.54 | 0.21 | | | | 0.11 | 0.971 |
| | 48 | 1.22 | 2.17 | 10.13 | 1.42 | | | | 0.13 | |
| | 72 | 0.99 | 1.52 | 9.77 | 0.63 | | | | 0.22 | |
| | 96 | 0.86 | 1.44 | 8.12 | 0.77 | 0.31 | -2.21 | 0.53 | 0.78 | |
| 2B | 24 | 0.73 | 1.97 | 7.46 | 0.84 | | | | 0.13 | 0.984 |
| | 48 | 2.31 | 3.22 | 16.52 | 1.09 | | | | 0.15 | |
| | 72 | 2.14 | 3.56 | 12.44 | 1.54 | | | | 0.24 | |
| | 96 | 1.98 | 2.94 | 10.12 | 0.13 | 1.02 | -1.82 | 0.62 | 0.84 | |
| 3B | 24 | 1.87 | 2.10 | 9.81 | 0.15 | | | | 0.10 | 0.976 |
| | 48 | 1.74 | 2.13 | 9.54 | 3.11 | | | | 0.19 | |
| | 72 | 0.44 | 4.18 | 19.46 | 2.56 | | | | 0.23 | |
| | 96 | 1.12 | 4.69 | 18.57 | 1.69 | 1.42 | -2.14 | 0.77 | 0.80 | |
| 4B | 24 | 2.98 | 4.36 | 18.11 | 2.31 | | | | 0.19 | 0.982 |
| | 48 | 1.56 | 0.81 | 10.64 | 1.43 | | | | 0.22 | |
| | 72 | 1.31 | 0.74 | 11.24 | 1.22 | | | | 0.27 | |
| | 96 | 0.31 | 3.71 | 17.14 | 0.46 | 1.72 | -2.43 | 0.84 | 0.91 | |

borne by the undamaged part of the rock mass; and $\sigma_2$ is the effective stress borne by the damaged part of the rock mass, which is defined as residual stress. Then, the damage variable is:

$$\begin{cases} D_m = \dfrac{A_3 - A_5}{A - A_4} & (a) \\ D_n = \dfrac{A_4}{A} & (b) \Rightarrow D = D_m + D_n - D_m D_n \\ D = \dfrac{A_3 + A_4 - A_5}{A} & (c) \end{cases} \tag{6}$$

where $D_m$ is the damage variable under the shear creep load, $D_n$ is the damage variable under the fatigue load, and $D$ is the total damage variable of the rock mass.

Assuming that the probability density function of rock failure obeys the Weibull distribution, the damage variable $D_m$ under the shear creep load can be expressed as:

$$D_m = 1 - \exp[-(\frac{F}{F_0})^m] \tag{7}$$

where $F$ is the microelement strength of the rock mass, $F_0$ and $m$ are both Weibull distribution parameters, $F_0$ is the reflection of the macrostatistical average strain strength of the rock mass, and $m$ is the reflection of the concentration of the microelement strain intensity distribution within the material.

The effect of fatigue loading degrades the macroscopic mechanical properties of rocks, and rock deformation can be used as a parameter to measure damage. The process of transforming from undisturbed dynamics to completely disturbed dynamics is usually expressed by the disturbance state equation $D_n$. Considering the damage and destruction of the specimen caused by fatigue disturbance, the damage variable $D_n$ is defined as (Kaya and Sayın 2017):

$$D_n = \frac{\varepsilon_2 - \varepsilon_1}{\varepsilon_1} = \frac{\varepsilon_2}{\varepsilon_1} - 1 \tag{8}$$

where $\varepsilon_1$ is the shear strain of the specimen without a fatigue load and $\varepsilon_2$ is the shear strain of the specimen with a fatigue load.

Thus, the total damage variable $D$ of the rock mass is obtained:

$$D = 1 - (\frac{\varepsilon_2}{\varepsilon_1} + 2)\exp[-(\frac{F}{F_0})^m] \tag{9}$$

Considering Lemaitre's strain equivalence assumption (Lemaitre 1984), the apparent stress needs to be transformed into effective stress, and the transformation is completed with the equation of state under the appropriate fatigue load, and the constitutive relationship of rock mass damage is obtained:

$$\sigma = (1\text{-}D)\sigma_0 \tag{10}$$

where $\sigma_0$ is the apparent stress and $\sigma$ is the effective stress. Then, the rheological constitutive equation of the anchored rock mass under creep-fatigue loading is as follows:

(1) When $t \le t_s$, the model is transformed into the linear model of the anchored rock mass in Fig. 6. After considering the effect of the creep-fatigue load, the attenuation of the shear creep of the anchored rock mass under the creep-fatigue load is obtained. In the steady state phase, the corresponding creep state equation is:

$$\varepsilon(t) = (1 - D) * [\frac{Q}{P} + \exp(-Pt) * (\frac{\sigma_0}{E_h + E_s} - \frac{Q}{P})] \tag{11}$$

(2) When $t > t_s$, the model is a nonlinear rheological model of the rock mass. After considering the effect of the

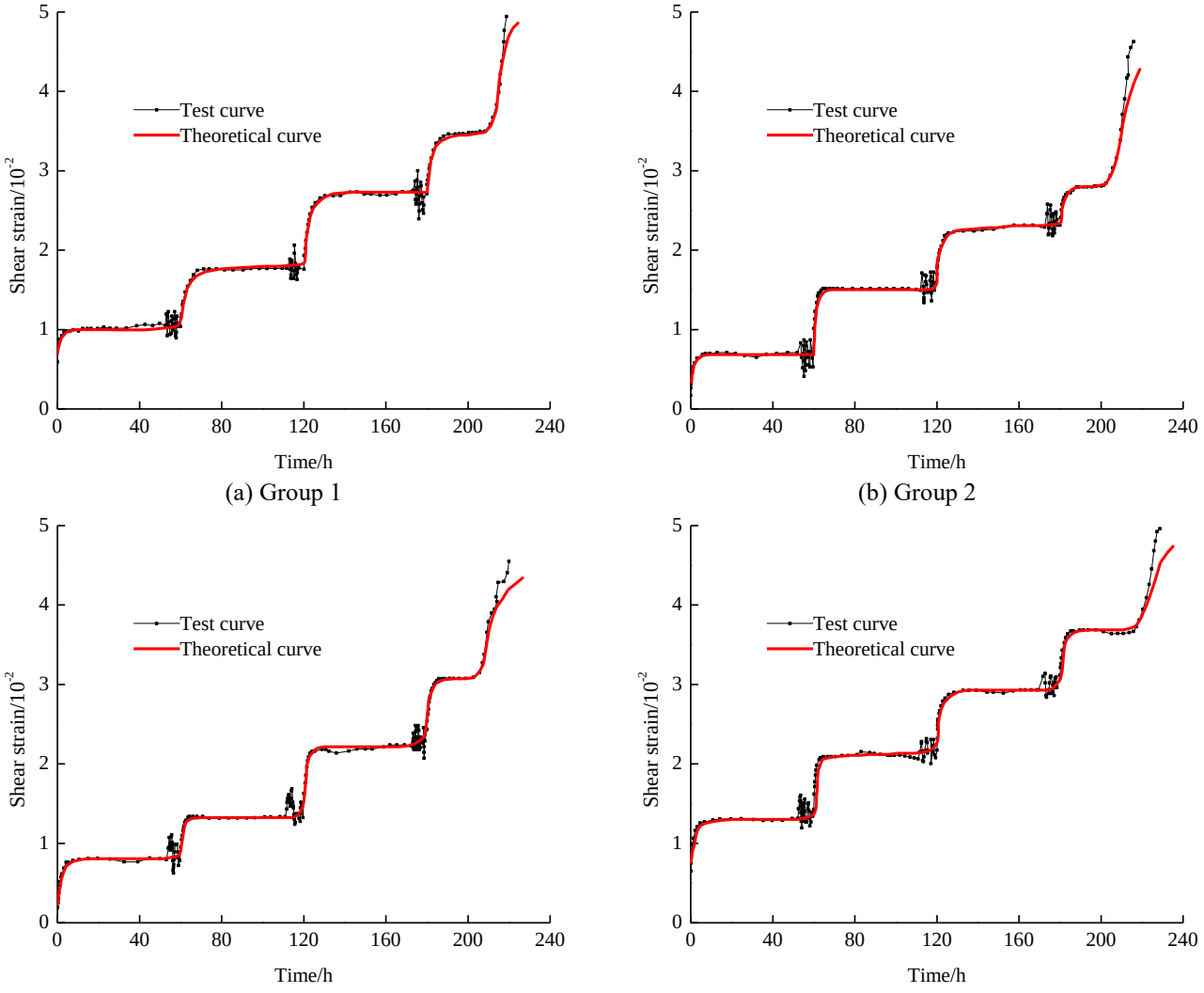


(a) Group 1 (b) Group 2

(c) Group 3 (d) Group 4

Fig. 10 Comparison of test data and fitting curve

creep-fatigue load, the entire process of shear creep of the anchored rock mass under the creep-fatigue load is obtained, including the acceleration phase. The corresponding creep state equation is:

$$\varepsilon(t)=(1-D)*[\frac{Q}{P}+\exp(-Pt)*(\frac{\sigma_0}{E_h+E_s}-\frac{Q}{P})]+D\frac{\sigma}{E_H}\{1-m\times\exp[-(\frac{t-t_s}{t_p-t_s})^n]\} \quad (12)$$

## 4. Parameter solving and analysis

### *4.1 Parameter solving and verification*

Based on the results of creep tests, accurate and reliable technical methods are used to identify the parameters in the creep model (Yang *et al.* 2007). In this paper, the mathematical optimization software 1st Opt based on the Broyden-Fletcher-Goldfarb-Shanno (BFGS) algorithm and the general global optimization method is used to describe the test group curve in Fig. 4, and the relevant parameters are shown in Table 5.

Putting the model parameters in Table 5 into Eq. (12), the shear creep equation of an anchored rock mass under creep-fatigue loading can be obtained, and the test curve can be drawn to compare with the theoretical curve, as illustrated in Fig. 10. Fig. 10 and Table 5 show that the theoretical curve of the nonlinear rheological model established in this paper is in good agreement with the laboratory test curve; the fitting coefficient $R^2$ is greater than 0.97, indicating that the rheological model can reflect the anchoring effect under creep-fatigue loading conditions. The whole process of rock mass shear deformation and failure is accurately captured by the model.

### *4.2 Model parameter analysis*

To study the influence of the acceleration factor $m$ and the failure factor $n$ of the nonlinear element parameters in the rheological model on the shear creep curve, the test data and model parameters with a shear stress of 96 MPa (numbered 1B in Table 5) are considered.

(1) Acceleration factor $m$

To study the influence of the acceleration factor $m$ on the shear creep curve and ensure that the other rheological model parameters remain unchanged, the strain-time curves

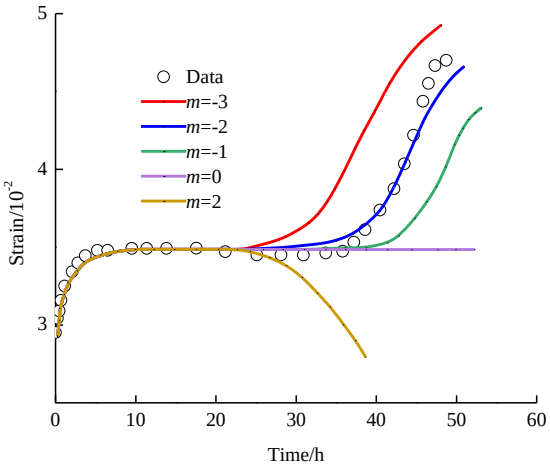


Fig. 11 Strain-time curves under different acceleration factors

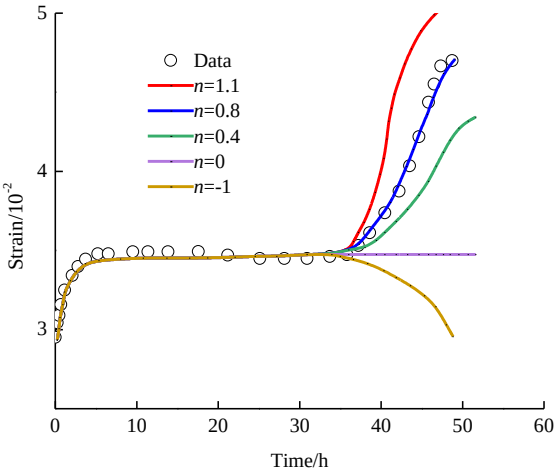


Fig. 12 Strain-time curves under different failure factors

under different acceleration factors $m$ are drawn, as shown in Fig. 11.

As shown in the figure above, (1) the strain is negatively correlated with the acceleration factor $m$. With the gradual increase in the acceleration factor $m$, the peak strain gradually decreases. (2) The acceleration factor $m$ has not only a negative effect on the acceleration stage of the creep curve but also a certain degree of influence on the latter half of the steady-state stage of the curve. (3) Additionally, when the acceleration factor $m<0$, it has no obvious influence on the shape of the strain-time curve in the acceleration stage, and the curve shows an overall translation phenomenon in the acceleration stage, with a limited influence on the peak strain. When $m=0$, the model can describe only the attenuation and steady-state stages, and the constitutive equation cannot describe the change in the acceleration stage. When $m>0$, the strain-time curve exhibits a sharp decline.

(2) Destruction factor $n$

To study the influence of the damage factor $n$ on the curve and ensure that the other rheological model parameters remain unchanged, the strain-time curves under different damage factors $n$ are drawn, as shown in Fig. 12:

As shown in the Fig. below, (1) the strain is positively correlated with the failure factor $n$. With the increase in the failure factor $n$, the peak strain gradually increases, and (2) the failure factor $n$ has a positive effect on only the acceleration stage of the creep curve and the steady state. The failure factor $n$ has no effect on the other stage of the curve. (3) Additionally, when the damage factor $n>0$, the damage factor will change only slightly, and the curve of the acceleration stage will undergo a larger change, which exponentially increases the change in strain during the acceleration stage. When $n=0$, there is no acceleration stage in the creep curve, so that the steady-state stage continues. When $n<0$, the theoretical curve decreases in the acceleration stage. Compared with that when $n>0$, this amplitude of decrease is smaller when $n$ is less than or equal to 0.

## 5. Conclusions

In this paper, through the comparison test results of the shear creep of marble with and without a fatigue load, the relevant conclusions are as follows:

• The shear creep characteristics of rock under creep-fatigue loading are obvious, and the peak strain of a rock mass under a creep-fatigue load is larger than the peak strain of a corresponding specimen under only a shear creep load, and the average strain is increased by 18.3%. The highest increase observed corresponds to the first group of tests, with an increase of 22%, and the lowest increase observed corresponds to the fourth group of tests, with an increase of 12.4%.

• From the shear strain-time test curve, when the first level of stress is applied, the two curves basically coincide whether a fatigue load is included. With increasing stress level, there is a creep-fatigue load test curve in which the strain increment increases, the strain difference among the specimens during the steady-state stage gradually increases, and the curve gap gradually increases. When the fourth level of stress is applied, the strain difference reaches the maximum.

• The parameter analysis of the accelerating element in the rheological model indicates that among the element parameters, the acceleration factor $m$ and the peak strain have a negative relationship while the damage factor $n$ has a positive relationship with the peak strain.

• The acceleration stage of the shear creep of an anchored rock mass is described by introducing an acceleration element and considering the damage and destruction under fatigue loading to obtain the creep that reflects the whole process of the shear creep of the anchored rock mass under a fatigue load. The results of the proposed fatigue model is verified with the results of indoor tests, providing a reference for rock stability research.

The author holds that the key scientific problem from the anchoring mechanism of the deep-jointed rock mass under the complex stress path has the characteristics of wide range, strong correlation with practical engineering, long research duration, and great difficulty in carrying out experiments. For a long time, many scholars at home and abroad have conducted a lot of research work on this direction, and have reached a certain consensus in some

aspects. However, due to the different emphasis of many researches, the research results are scattered, and lack representativeness. In this paper, the shear mechanical characteristics of the anchored rock mass under the creep fatigue load are analyzed. Furthermore, abundant significant conclusions are obtained based on the self-study. However, the following problems still need to be further studied: (1) the mechanical properties of the deep rock mass under the complex path are mainly studied, and the reinforcement mechanism on bolts to structural plane is discussed; (2) the prestress of the anchored rock mass under the complex stress path is studied. (3) The interaction and deformation law among bolt, rock mass, and joint surface is explored. The solution of the above-mentioned problems is of great significance for the in-depth study on the anchoring mechanism of the deep jointed rock mass under the complex stress paths, and for guiding the construction.

## Acknowledgments

The research described in this paper was financially supported by the National Natural Science Foundation (51974146), Liaoning Natural Science Foundation (2019-ZD-0042) and Discipline Innovation team of Liaoning Technical University (LNTU20TD08).

## References

Ajamzadeh, M., Sarfarazi, V. and Dehghani, H. (2019), "Evaluation of plow system performance in long-wall mining method using particle flow code", *Int. J. Coal Sci. Technol.*, **6**(4), 518-535. https://doi.org/10.1007/s40789-019-00266-3.

Bagde, M.N. and Petroš, V. (2005), "Waveform effect on fatigue properties of intact sandstone in uniaxial cyclical loading", *Rock Mech. Rock Eng.*, **38**(3), 169-196. https://doi.org/10.1007/s00603-005-0045-8.

Chen, G., Chen, T., Chen, Y., Huang, R. and Liu, M. (2018), "A new method of predicting the prestress variations in anchored cables with excavation unloading destruction", *Eng. Geol.*, **241**, 109-120. https://doi.org/10.1016/j.enggeo.2018.05.015.

Chen, L., Wang, E., Junjun, F., Li, X., Kong, X. and Zhang, Z. (2016), "Numerical simulation on gas continuous emission from face during roadway excavation", *Geomech. Eng.*, **10**(3), 297-314. https://doi.org/10.12989/gae.2016.10.3.297.

Choi, S.G., Chu, J. and Kwon, T.H. (2019), "Effect of chemical concentrations on strength and crystal size of biocemented sand", *Geomech. Eng.*, **17**(5), 465-473. https://doi.org/10.12989/gae.2019.17.5.465.

Griggs, D. (1939), "Creep of rocks", *J. Geol.*, **47**(2), 225-251. https://doi.org/10.1086/624775.

Jiang, Z., Jiang, Z., Li, H. and Wang, S. (2017), "Creep-seepage coupling laws of quartzite under cyclic loading-unloading conditions", *Chin. J. Geotech. Eng.*, **39**(10), 1832-1841. https://doi.org/10.11779/CJGE201710011.

Jorat, M.E., Kreiter, S., Mörz, T., Moon, V. and de Lange, W. (2013), "Strength and compressibility characteristics of peat stabilized with sand columns", *Geomech Eng*, **5**(6), 575-594. https://doi.org/10.12989/gae.2013.5.6.575.

Kaya, A. and Sayın, A. (2017), "Engineering geological appraisal and preliminary support design for the Salarha Tunnel, Northeast Turkey", *B. Eng. Geol. Environ.*, **78**(2), 1095-1112. https://doi.org/10.1007/s10064-017-1177-2.

Kılıc, A., Yasar, E. and Atis, C.D. (2003), "Effect of bar shape on the pull-out capacity of fully-grouted rockbolts", *Tunn. Undergr. Sp. Tech.*, **18**(1), 1-6. https://doi.org/10.1016/S0886-7798(02)00077-9.

Kılıc, A., Yasar, E. and Celik, A.G. (2002), "Effect of grout properties on the pull-out load capacity of fully grouted rock bolt", *Tunn. Undergr. Sp. Tech.*, **17**(4), 355-362. https://doi.org/10.1016/S0886-7798(02)00038-X.

Lemaitre, J. (1984), "How to use damage mechanics", *Nucl. Eng. Des.*, **80**(2), 233-245. https://doi.org/10.1016/0029-5493(84)90169-9.

Liu, J. and Li, J. (2018), "Analysis on meso-damage characteristics ofmarble under triaxial cyclic loading and unloading based on particle flow simulation", *J. Cent. South Univ. Nat. Sci. Ed.*, **49**(11), 2797-2803. https://doi.org/10.11817/j.issn.1672-7207.2018.11.021.

Meng, Q., Zhang, M., Han, L., Pu, H. and Nie, T. (2016), "Effects of acoustic emission and energy evolution of rock specimens under the uniaxial cyclic loading and unloading compression", *Rock Mech. Rock Eng.*, **49**(10), 3873-3886. https://doi.org/10.1007/s00603-016-1077-y.

Nield, J.M., King, J. and Jacobs, B. (2014), "Detecting surface moisture in aeolian environments using terrestrial laser scanning", *Aeolian Res.*, **12**, 9-17. https://doi.org/10.1016/j.aeolia.2013.10.006.

Scheuermann, A. (1978), "Suggested methods for determining the strength of rock materials in triaxial compression", *Int. J. Rock Mech. Min. Sci. Gcomech. Abstr.*, **15**(2), 47-51. https://doi.org/10.1016/0148-9062(78)91677-7.

Song, Y., Li, Y., Wang, W. and Liu, J. (2020), "Shear creep characteristics and constitutive model analysis of jointed rock mass", *J. China Coal Soc.*, **45**(4), 1357-1366. https://doi.org/10.13225/j.cnki.jccs.2019.1428.

Tadeusiewicz, R. (2015), "Neural networks in mining sciences – General overview and some representative examples", *Arch Min Sci*, **60**(4), 971-984. https://doi.org/10.1515/amsc-2015-0064.

Tang, L., Zhao, Z., Chen, H., Wu, Y. and Zeng, Y. (2019), "Dynamic stress accumulation model of granite residual soil under cyclic loading based on small-size creep tests", *J. Cent. South Univ.*, **26**(3), 728-742. https://doi.org/10.1007/s11771-019-4043-5.

Vásárhelyi, B. and Ván, P. (2006), "Influence of water content on the strength of rock", *Eng. Geol.*, **84**(1), 70-74. https://doi.org/10.1016/j.enggeo.2005.11.011.

Wang, J., Fu, J. and Song, W. (2020), "Mechanical properties and microstructure of layered cemented paste backfill under triaxial cyclic loading and unloading", *Constr. Build. Mater.*, **257**, 119540. https://doi.org/10.1016/j.conbuildmat.2020.119540.

Wang, J., Liang, B. and Yang, P. (2019), "Creep experiment and nonlinear disturbance creep model of gneiss under dynamic and static loads", *J. China Coal. Soc.*, **44**(1), 192-198. https://doi.org/10.13225/j.cnki.jccs.2018.5036.

Wang, J., Ning, J., Qiu, P., Yang, S. and Shang, H. (2019), "Microseismic monitoring and its precursory parameter of hard roof collapse in longwall faces: A case study", *Geomech. Eng.*, **17**(4), 375-383. https://doi.org/10.12989/gae.2019.17.4.375.

Xu, P. and Yang, S. (2015), "Study of visco-elasto-plastic constitutive model of coal under cyclic loading", *Chin. J. Rock Mech. Eng.*, **34**(3), 537-545. https://doi.org/10.13722/j.cnki.jrme.2015.03.011.

Xue, Y., Kong, F., Yang, W., Qiu, D., Su, M., Fu, K. and Ma, X. (2020), "Main unfavorable geological conditions and engineering geological problems along Sichuan-Tibet railway", *Chin. J. Rock Mech. Eng.*, **39**(3), 445-468. https://doi.org/10.13722/j.cnki.jrme.2019.0737.

Yang, S., Xu, W. and Yang, S. (2007), "Investigation on shear rheological mechanical properties of shale in Longtan

Hydropower Project", *Rock Soil Mech*., **28**(5), 47-54. https://doi.org/10.16285/j.rsm.2007.05.009.
Yang, X., Han, X., Liu, E., Zhang, Z. and Wang, X. (2018), "Experimental study on the acoustic emission characteristics of non-uniform deformation evolution of granite under cyclic loading and unloading test", *Rock Soil Mech*., **39**(8), 2732-2739. https://doi.org/10.16285/j.rsm.2018.0048.

*CC*